SCIENCE CHINA
Technological Sciences

•Article•

January 2019 Vol.62 No.1: 60–69
https://doi.org/10.1007/s11431-017-9300-5

Low frequency vibration control of railway vehicles based on a high static low dynamic stiffness dynamic vibration absorber

SUN Yu, GONG Dao*, ZHOU JinSong, SUN WenJing & XIA ZhangHui

Institute of Rail Transit, Tongji University, Shanghai 201804, China

Received December 25, 2017; accepted June 4, 2018; published online November 29, 2018

In order to control the low frequency vibration of railway vehicles, a vertical two degrees of freedom (2DOF) low frequency dynamic vibration absorber (DVA) based on acceleration is proposed. Parameters of the dynamic vibration absorber are put forth to control the low frequency vibration of car body bouncing and pitching. Next, the acceleration power spectrum density (PSD) and ride quality of the car body are calculated based on the pseudo excitation method (PEM) and covariance algorithm, respectively. According to the requirement of 2DOF low frequency DVA, the isolators with high static low dynamic stiffness (HSLDS) are designed. A high-speed train dynamic model containing HSLDS isolators is established to validate the effects on the car body vibration. The results reveal that the 2D low frequency DVA can significantly reduce the vibration of the car body bouncing and pitching. Thus, the ride quality of the vehicle is increased, and passenger comfort is improved.

railway vehicle dynamics, ride quality, low frequency, dynamic vibration absorber, high static low dynamic stiffness

Citation: Sun Y, Gong D, Zhou J S, et al. Low frequency vibration control of railway vehicles based on a high static low dynamic stiffness dynamic vibration absorber. Sci China Tech Sci, 2019, 62: 60–69, https://doi.org/10.1007/s11431-017-9300-5

1 Introduction

Ever-increasing train running speeds have resulted in increases in running vibration and decreases in riding comfort. It is necessary to investigate ways to improve riding comfort by considering the influence of vibration on human physiology. When a person remains in an environment of vibration for any length of time, fatigue is caused along with resonance between internal organs, whole-body, and the external environment. Some scholars have studied vibration control through the external environment such as track and pantograph [1,2] to solve these problems, while others study the vibration control of the vehicle body itself. Zhou et al. [3,4] developed a comprehensive performance analysis method for vehicle dynamic features based on modal parameters. The relationship between dynamic parameters, physical parameters, and riding comfort is established based on a track-vehicle-human model to investigate the low frequency vibration of vehicles. By regarding the car body as a homogeneous Euler beam, a rigid-flexible coupling vertical dynamic model comprising structural damping and DVA is developed. The influence of DVA on inhibiting car body elastic vibration is studied based on the covariance algorithm. Gong et al. [5–7] proposed a full modal calculation method for the elastic body based on the Green function. By taking advantages of the vehicle rigid-flexible coupling vibration analytical model considering elasticity, the full-band vibration features of the elastic car body are analyzed. By regarding the car body as a homogeneous Euler beam supported by secondary suspension and installing DVA in the underbody, the inhibition effect of DVA on car body elasticity is analyzed, implying that the DVA can effectively reduce the elastic vibration. Shi et al. [8] apply DVA theory to restrain the elastic vibration of carbody for high-speed electric multiple unit, and optimize the parameters of the DVA. Dumitriu [9] proposes anti-bending bars which are

*Corresponding author (email: gongdao@tongji.edu.cn)

fixed onto the longitudinal beams of a car body underframe to suppress the elastic vibration of the car body.

In previous studies on car body vibration control, the majority have focused on the inhibition of elastic vibration, while few thought to control the rigid vibration. For the vertical vibration of the car body, the elastic vibration is generally concentrated in the vicinity of 10 Hz, the rigid vibration concentrated below 2 Hz, according to the ride comfort for the evaluation of the stability of the weight function can be known [10], the rigid vibration control has a more important significance than elastic vibration control. This paper focuses on finding a way to control the rigid vibration of railway vehicle car body.

The research of low frequency vibration control is limited by the development of vibration isolator. For the traditional linear vibration isolator, the isolation frequency is in contradiction with static deflection. To solve this problem, high static and low dynamic stiffness (HSLDS) isolator is proposed. Carrella et al. [11–13] place a pair of linear springs horizontally to generate negative stiffness in the vertical direction, and by multiplying it with vertical linear springs, a vibration isolation system with HSLDS is obtained. When the equivalent linear system has the same static deflection, the system has a lower natural frequency. Huang et al. [14–16] obtain an ultralow-frequency nonlinear vibration isolation system by multiplying a knife-edge supporting sliding beam with negative stiffness and linear springs with positive stiffness. They also develop a vibration isolator with quasi-zero stiffness by multiplying a Euler buckling beam structure with negative stiffness and a linear vibration isolator. Palomares et al. [17] present a HSLDS system based on a set of two double-acting pneumatic linear actuators, and investigate its vibration isolation performance by experimental tests and simulations. Meng et al. [18,19] construct quasi-zero-stiffness vibration isolators by multiplying disc springs with equal/variable thickness values and linear springs. By investigating their static and dynamic features, the influences of parameters including excitation amplitude, mass ratio, and damping ratio on the disc spring quasi-zero-stiffness vibration isolators are obtained. However, the research on HSLDS mostly studies the theory of isolator and seldom studies on engineering application. The characteristics of the HSLDS vibration isolator solves the conflict between the dynamic stiffness and static deflection of the traditional linear vibration isolator, and it can be used to control the rigid vibration of railway vehicle car body.

In this paper, a 2 degrees of freedom (DOF) DVA capable of controlling car body bouncing and pitching simultaneously are developed in order to control the low frequency virabtion of railway vehicles. By utilizing the PEM and ride quality covariance method, the influences of the 2 DOF DVA on car body vibration during the operating conditions of railway vehicle are calculated. As for the low dynamic stiffness suspension isolators required in the 2 DOF DVA, this study develops a novel isolator with HSLDS by connecting rubber springs to disc springs which is of negative stiffness. Using multibody system simulation tool SIMPACK, a nonlinear vehicle dynamic model containing these novel isolators is constructed to analyze their influence on car body vibration.

2 Mechanism of 2DOF DVA based on acceleration

As essential damping devices for vibration control, DVAs have been widely applied in a myriad of fields including architecture and machinery [20,21]. A DVA consists of assistant mass, springs, and dampers. Its working principle is to take advantage of the anti-resonance features of mutiple degrees-of-freedom systems. When the main system vibrates, the DVA also vibrates. Due to the dynamic effect of the DVA, the force applied on the main system is opposite to the external excitation force, and the combined force applied on the main system is reduced. Thereby, the vibration of the main system is reduced.

Figure 1 shows a DVA that considers both bouncing and pitching of the main vibration system where m_1 and J_1 are the mass and rotational inertia of the main vibration system, respectively, and m_2 and J_2 are the mass and rotational inertia of the DVA, respectively. It is worth noting that the damping of the main system is not considered in Figure 1 which has little effect on the DVA design [3,5,18]. The dynamics vibration differential equation of the system can be obtained as

$$m_1\ddot{x}_1 = -2k_1x_1 - 2k_2(x_1 - x_2) - 2c(\dot{x}_1 - \dot{x}_2) + F_1e^{i\omega t}, \quad (1)$$

$$m_2\ddot{x}_2 = -2k_2(x_2 - x_1) - 2c(\dot{x}_2 - \dot{x}_1), \quad (2)$$

$$J_1\ddot{\theta}_1 = -2k_1l_1^2\theta_1 - 2k_2l_2^2(\theta_1 - \theta_2) - 2cl_2^2(\dot{\theta}_1 - \dot{\theta}_2) + T_1e^{i\omega t}, \quad (3)$$

$$J_2\ddot{\theta}_2 = -2k_2l_2^2(\theta_2 - \theta_1) - 2cl_2^2(\dot{\theta}_2 - \dot{\theta}_1), \quad (4)$$

where x_1, θ_1, k_1, and l_1 are the vertical displacement, pitching angle, suspension stiffness, and half of the suspension span of the main vibration system, respectively. x_2, θ_2, k_2, c, and l_2 are the vertical displacement, pitching angle, suspension stiffness, damping, and half of the support span of the DVA, respectively. F_1 and T_1 are the amplitudes of force and torque applying on the main vibration system, respectively. According to the vibration differential equation of the model, it is found that the bouncing and pitching are independent without coupling. Hence, these two vibration modes can be described individually. The pitching vibration is taken as an example in this research. The pitching DVA mechanism based on acceleration is deduced with dynamics eqs. (3) and (4). By combining these two equations, the solution is as-

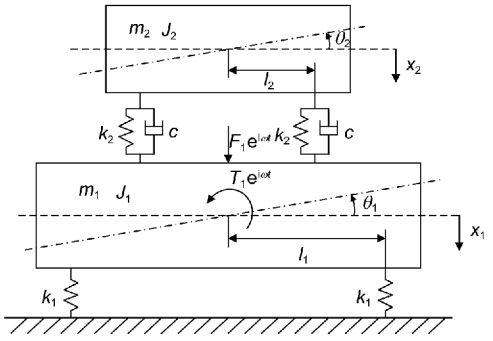

Figure 1 (Color online) A schematic diagram of 2DOF DVA.

sumed as

$$\theta_1(t) = \Theta_1 e^{i(\omega t-\phi)}, \quad \theta_2(t) = \Theta_2 e^{i(\omega t-\phi)}, \tag{5}$$

where Θ_1 and Θ_2 are the response amplitudes of the main vibration system and the DVA, respectively, and ϕ is the phase. The acceleration of the main vibration system is expressed as

$$\ddot{\theta}_1(t) = -\omega^2\Theta_1 e^{i(\omega t-\phi)} = A_1 e^{i\omega t}, \tag{6}$$

where A_1 is a complex number containing the amplitude and phase information of the acceleration. eqs. (5) and (6) are substituted into eqs. (3) and (4) with $\omega_1 = \sqrt{2k_1 l_1^2/J_1}$, $\omega_2 = \sqrt{2k_2 l_2^2/J_2}$, $\theta_{st} = T_1/(2k_1 l_1^2)$, $\mu = J_2/J_1$, $\beta = \omega_2/\omega_1$, $\lambda = \omega/\omega_1$, and $\zeta = cl_2^2/(J_2\omega_1)$ are introduced. Among them, ω_1 is the natural angular frequency of the main vibration system, ω_2 is the natural angular frequency of the DVA, θ_{st} is the static deformation of the main vibration system, μ is the rotational inertia ratio, β is the natural angular frequency ratio of the DVA to the main vibration system, λ is the forced vibration frequency ratio, and ζ is the damping ratio. After data collation, the amplification factor of the main system's pitching acceleration can be obtained as

$$\left|\frac{A_1}{\theta_{st}}\right| = \sqrt{\frac{\lambda^4\left[(\beta^2-\lambda^2)^2+(2\zeta\lambda)^2\right]}{\left[(1-\lambda^2)(\beta^2-\lambda^2)-\mu\beta^2\lambda^2\right]^2+(2\zeta\lambda)^2(1-\lambda^2-\mu\lambda^2)^2}}. \tag{7}$$

Based on the fixed-point theory, the coordinates of fixed-points P and Q are acquired by setting $\zeta = 0$ and $\zeta = \infty$ as equal. The optimal value β of the DVA based on acceleration response can be acquired as

$$\beta = \frac{1}{\sqrt{1+\mu}}. \tag{8}$$

Figure 2 shows the relation between the fixed-points (P and Q) and acceleration response of the main vibration system when the optimal value β based on acceleration response are satisfied. The figure demonstrates the state of $\mu = 0.1$, with $\zeta = 0.18$ as the optimal damping of the DVA. At that moment, the peak value of the acceleration response amplitude ratio of the main vibration system positioned around points P and Q.

3 Establishment and analysis of the linear vertical dynamics vehicle model

3.1 Establishment of the vehicle vertical linear dynamics model

Vehicle model establishment is typically conducted individually since weak coupling exists between the vertical and lateral dynamics of railway vehicles. A high-speed train vehicle vertical dynamics model is developed in this study shown in Figure 3. During vehicle running, the wheels are assumed to tightly contact the steel track, and the vertical motion equations of the wheelsets are not considered during model establishment. The model has eight degrees of freedom, which includes the bouncing and pitching motions of the car body, DVA, leading bogie, and trailing bogie (2×4).

According to the vehicle dynamic model displayed in Figure 3, dynamics equations are listed as follows:

$$\begin{aligned} m_b\ddot{z}_b = &-2k_s z_b + k_s z_{t1} + k_s z_{t2} + -2c_s\dot{z}_b + c_s\dot{z}_{t1} \\ &+c_s\dot{z}_{t2} - k_e(2z_b - 2z_e) - c_e(2\dot{z}_b - 2\dot{z}_e), \end{aligned} \tag{9}$$

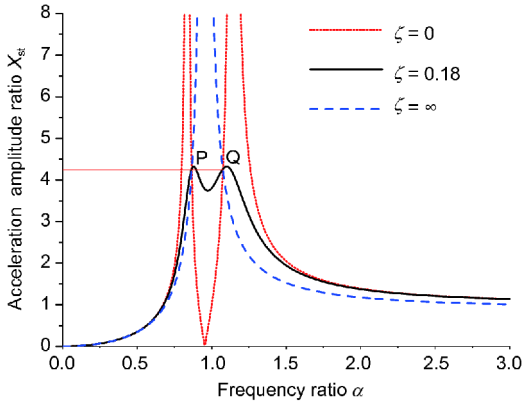

Figure 2 (Color online) Acceleration response curves of the main vibration system.

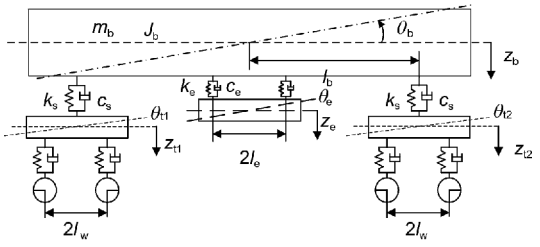

Figure 3 Vertical dynamics model of a high-speed train vehicle.

$$J_b\ddot{\theta}_b = -2k_s l_b^2\theta_b - k_s l_b z_{t1} + k_s l_b z_{t2} - 2c_s l_b^2\dot{\theta}_b - c_s l_b\dot{z}_{t1} + c_s l_b\dot{z}_{t2} - k_e(2l_e\theta_b - 2l_e\theta_e)l_e - c_e(2l_e\dot{\theta}_b - 2l_e\dot{\theta}_e)l_e, \quad (10)$$

$$m_t\ddot{z}_{t1} = -(k_s + 2k_p)z_{t1} + k_s z_b - k_s l_b\theta_b + c_s\dot{z}_b - c_s l_b\dot{\theta}_b - (c_s + 2c_p)\dot{z}_{t1} + c_p\dot{z}_{w1} + c_p\dot{z}_{w2} + k_p z_{w1} + k_p z_{w2}, \quad (11)$$

$$J_t\ddot{\theta}_{t1} = -2k_p l_w^2\theta_{t1} - k_p l_w z_{w1} + k_p l_w z_{w2} - 2c_p l_w^2\dot{\theta}_{t1} - c_p l_w\dot{z}_{w1} + c_p l_w\dot{z}_{w2}, \quad (12)$$

$$m_t\ddot{z}_{t2} = -(k_s + 2k_p)z_{t2} + k_s z_b + k_s l_b\theta_b + c_s\dot{z}_b + c_s l_b\dot{\theta}_b - (c_s + 2c_p)\dot{z}_{t2} + c_p\dot{z}_{w3} + c_p\dot{z}_{w4} + k_p z_{w3} + k_p z_{w4}, \quad (13)$$

$$J_t\ddot{\theta}_{t2} = -2k_p l_w^2\theta_{t2} - k_p l_w z_{w3} + k_p l_w z_{w4} - 2c_p l_w^2\dot{\theta}_{21} - c_p l_w\dot{z}_{w3} + c_p l_w\dot{z}_{w4}, \quad (14)$$

$$m_e\ddot{z}_e = -k_e(2z_e - 2z_b) - c_e(2\dot{z}_e - 2\dot{z}_b), \quad (15)$$

$$J_e\ddot{\theta}_e = -k_e(2l_e\theta_e - 2l_e\theta_b)l_e - c_e(2l_e\dot{\theta}_e - 2l_e\dot{\theta}_b)l_e. \quad (16)$$

The parameters are derived from a typical high-speed train of China, and their meanings are summarized in Table 1.

By writing the above equation into a compact form, the following equation is obtained:

$$M\ddot{Z} + C\dot{Z} + KZ = D_w Z_w, \quad (17)$$

in which

$$Z = \left[z_b \quad \theta_b \quad z_{t1} \quad \theta_{t1} \quad z_{t2} \quad \theta_{t2} \quad z_e \quad \theta_e\right]^T, \quad (18)$$

$$Z_w = \left[z_{w1} \quad \dot{z}_{w1} \quad z_{w2} \quad \dot{z}_{w2} \quad z_{w3} \quad \dot{z}_{w3} \quad z_{w4} \quad \dot{z}_{w4}\right]^T, \quad (19)$$

where M is the mass matrix, C is the damping matrix, K is the stiffness matrix, and D_w is the excitation input matrix. By rewriting eq. (17) into an equation of state, the following can be obtained:

$$\dot{X} = AX + BZ_w, \quad (20)$$

where

$$X = \begin{bmatrix} Z \\ \dot{Z} \end{bmatrix}, \ A = \begin{bmatrix} 0 & I \\ -M^{-1}K & -M^{-1}C \end{bmatrix}, \ B = \begin{bmatrix} 0 \\ M^{-1}D_w \end{bmatrix}. \quad (21)$$

Table 2 shows the vibration frequency and damping ratio of the vehicle car body without DVA. The frequencies of car body bouncing and pitching are used as the target vibration absorbing frequencies of the DVA. This study uses high-

Table 1 Vehicle parameters and their meanings

Parameters	Units	Values	Meanings
m_b	t	39	Car body mass
J_b	t m^2	1744	Car body pitching rotational inertia
m_t	t	2624	Framework mass
J_t	t m^2	1047	Framework pitching rotational inertia
m_e	t	6	DVA mass
J_e	t m^2	47	DVA pitching rotational inertia
k_s	kN/m	192	Secondary vertical stiffness (per bogie side)
c_s	kN·s/m	10	Secondary vertical damp (per bogie side)
k_p	kN/m	1280	Primary vertical stiffness (per axle box)
c_p	kN s/m	13	Primary vertical damping coefficient (per axle box)
k_e	kN/m	47	DVA suspension stiffness (per side)
c_e	kN s/m	8	DVA suspension damping (per side)
l_b	m	8.9	Half of bogie distance
l_w	m	1.25	Half of axle distance
l_e	m	2	Half of absorber span

Table 2 Car body vibration modal frequency and damping ratio without DVA

Order	Vibration mode	Frequency (Hz)	Damping ratio (%)
1	Car body bouncing	0.6782	10.51
2	Car body pitching	0.8992	13.98
3	Bogie reverse bouncing	6.9271	30.74
4	Bogie homonymous bouncing	6.9343	30.61
5	Leading bogie pitching	12.3947	45.41
6	Trailing bogie pitching	12.3947	45.41

speed high excitation spectrum as track irregularity [22]. The PSD of the track irregularity is shown in Figure 4.

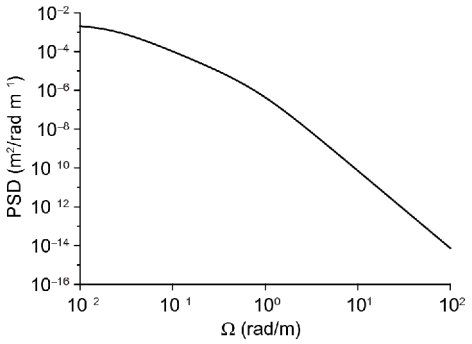

Figure 4 PSD of the track irregularity.

3.2 Analysis of vehicle vertical vibration

By referring to the parameters listed in Table 1 and track irregularity in Figure 4, dynamics analysis of the developed model is conducted by PEM [23,24]. Figure 5(a) and (b) illustrate the acceleration PSD at the car body bouncing and pitching with and without the 2DOF DVA during the vehicle running velocity of 350 km/h. As shown in Figure 5(a), after adopting the 2DOF DVA, the main frequency of the car body bouncing vibration changes from the original single-peak value to a double-peak value, and the peak value at the original bouncing vibration frequency (0.6782 Hz) decreases dramatically. Figure 5(b) shows that after adopting the 2DOF DVA, the peak value of the car body pitching vibration is slightly decreased.

Figure 6(a) and (b) give the vertical acceleration response PSD at the leading bogie and trailing bogie of the car body with and without the 2DOF DVA during the vehicle running velocity of 350 km/h. Whether at the leading bogie or the trailing bogie, the resonance peaks at the low-frequency points all change from single-peak values to double-peak values with obviously reduced vibration peak values after adopting the 2DOF DVA. This is attributed to the simultaneous reduction of the car body bouncing and pitching vibration after adopting the 2DOF DVA.

By ride quality covariance method [3], the Sperling indexes at the car body middle, above the leading bogie, and trailing bogie with and without the 2DOF DVA are calculated, which are shown as Figure 7(a)–(c) respectively. The ride quality Sperling index of the vehicle car body middle is only determined by the bouncing vibration, while the ride quality Sperling indexes at the leading bogie and the trailing bogie are determined by the superposition of the car body bouncing and pitching vibrations. It can be seen from the

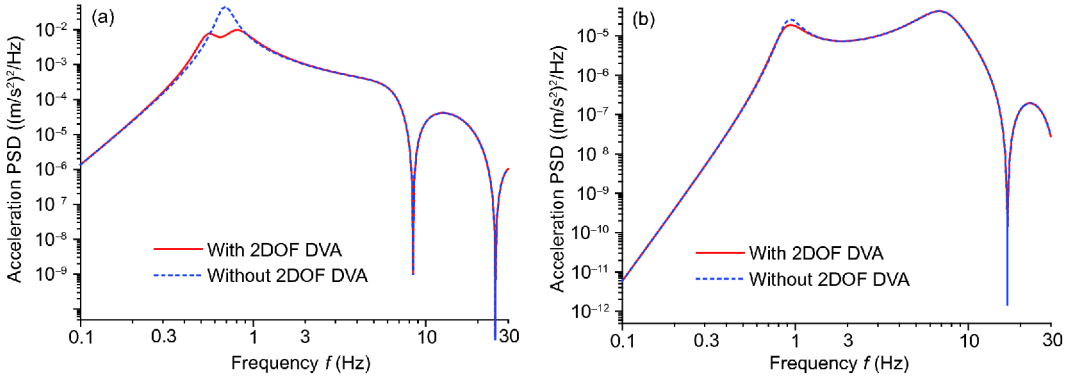

Figure 5 (Color online) (a) Acceleration PSD of the bouncing vibration mode; (b) acceleration PSD of the pitching vibration mode.

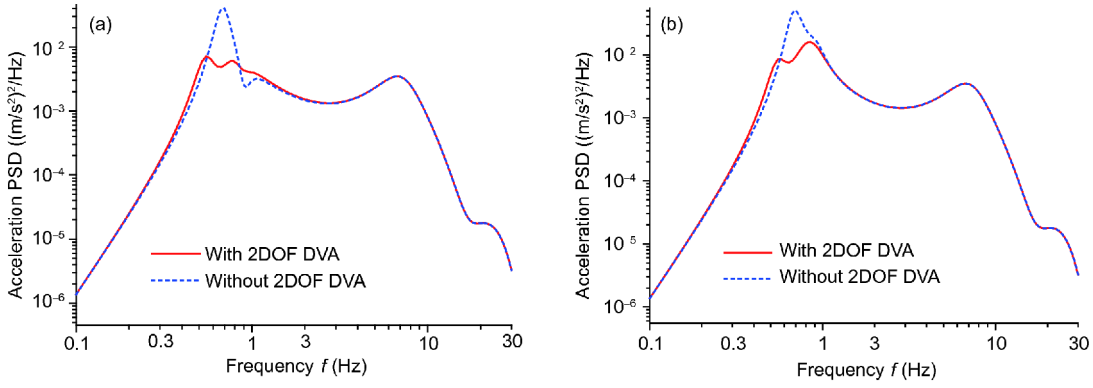

Figure 6 (Color online) (a) Acceleration PSD at the car body above leading bogie; (b) acceleration PSD at the car body above trailing bogie.

figure that after adopting the 2DOF DVA, the Sperling indexes at the car body middle, leading bogie, and trailing bogie during different running velocities all decreased significantly. The Sperling index of the car body above the trailing bogie will bigger than 2.5 if without the 2D DVA, which means not in an optimal level. When the running velocity is 400 km/h, the car body middle, leading bogie, and trailing bogie experience reduction of 0.273, 0.123, 0.136. This is attributed to the fact that the car body bouncing and pitchding are reduced by the 2DOF DVA. Thus, the low-frequency vibration acceleration amplitude of the car body decreases and the ride quality is improved.

3.3 Analysis of mass ratio and inertia ratio of 2DOF DVA

Figure 8(a) shows at the velocity of 350 km/h, the response conditions of the car body bouncing vibration acceleration PSD under different ratios of 2DOF DVA mass to car body mass μ_{m}. With the increase of mass ratio, the car body bouncing vibration acceleration PSD peak value decreases, and the inhibition frequency bandwidth increases. When the mass ratio is 0.1, the car body bouncing vibration acceleration PSD is decreased by 96.7% compared to that without 2DOF DVA. Figure 8(b) illustrates the response conditions of the car body pitching vibration acceleration PSD under different ratios of DVA pitching inertia to car body pitching inertia μ_{J}. The peak value of the pitching acceleration PSD at the pitching vibration mode frequency point decreases with the increase of inertia ratio. When the inertia ratio is 0.1, the peak value at the pitching vibration modal frequency point is 58.5% lower than that without 2DOF DVA.

4 Design of a HSLDS isolator

If conventional rubber isolators are used as the suspension isolators of the DVA. For a DVA with mass m, suspension stiffness k_{z}, suspension frequency f_{z}, and static deflection δ_{st}, the relationship of these parameters are

$$f_{\mathrm{z}}=\frac{1}{2\pi}\sqrt{\frac{k_{\mathrm{z}}}{m}},\ \delta_{\mathrm{st}}=\frac{mg}{k_{\mathrm{z}}}=\frac{g}{(2\pi f_{\mathrm{z}})^2}. \tag{22}$$

It indicates that the suspension frequency directly determines the suspension stiffness and static deflection. If the suspension frequency is too low, the static deflection of the absorber becomes over-sized, leading to problems like limitation bounds. According to previous analysis, for the 2DOF DVA to reduce the car body bouncing and pitching vibrations, the natural frequency of bouncing and pitching is about

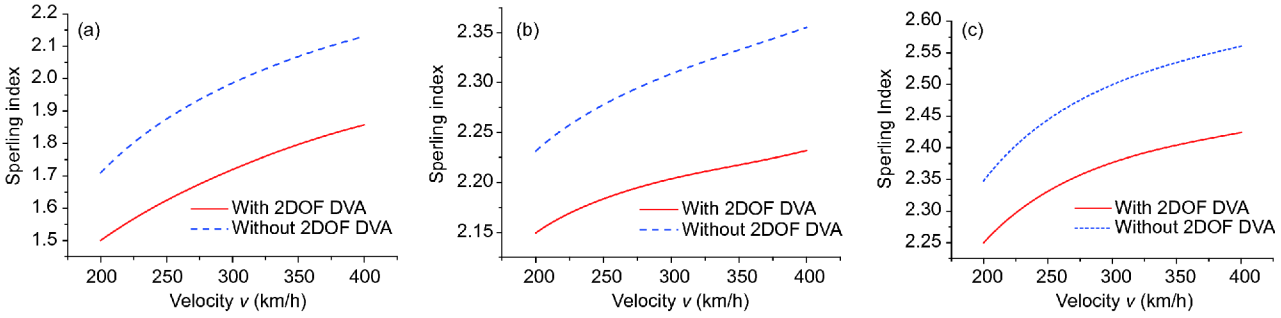

Figure 7 (Color online) (a) Sperling index at the car body middle; (b) sperling index at the car body above leading bogie; (c) sperling index at the car body above trailing bogie.

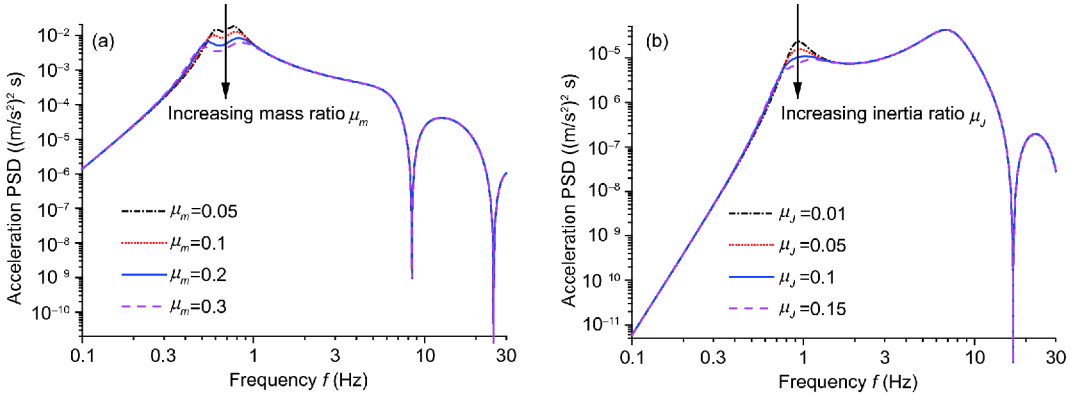

Figure 8 (Color online) (a) The relation between mass ratio and car body bouncing vibration; (b) the relation between mass ratio and car body pitching vibration.

1 Hz. It is unpractical to use only conventional rubber isolators as suspension isolators. Hence, in this paper, based on the negative stiffness feature of the disc spring, a HSLDS isolator is designed based on the parallel connection between a disc spring and a conventional rubber. Thus, the static deflection can be controlled when the 2DOF DVA is suspended in low frequency.

According to the difference of height-to-thickness ratio, disc springs present various loading features. When the height-to-thickness ratio is greater than $\sqrt{2}$, a segment of negative stiffness occurr (an area with negative curve slope), as displayed in Figure 9. The HSLDS isolator in this study is designed according to this feature of disc springs, as schematically shown in Figure 10.

The cross-section of an unsupported disc spring is shown in Figure 11, in which t_c is the thickness, h_0 is the initial height, D is the outer diameter, and d is the inner diameter. Usually, the loading force F_d of an unsupported disc spring (with an outer-to-inner diameter ratio of $C = 1, 2, 3, 4$) can be expressed as [25]

$$F_d = \frac{4E}{(1-\mu^2)} \cdot \frac{t_c^4}{K_1 D^2} \cdot \frac{x}{t_c} \times \left[\left(\frac{h_0}{t_c} - \frac{x}{t_c} \right) \left(\frac{h_0}{t_c} - \frac{x}{2t_c} \right) + 1 \right]. \tag{23}$$

where E is the elastic modulus, μ is the Poisson's ratio, x is the displacement generated from the initial position along the vertical direction of the disc spring, and K_1 is related to the outer-to-inner diameter ratio C ($C = D/d$).

$$K_1 = \frac{1}{\pi} \cdot \frac{\left(\frac{C-1}{C} \right)^2}{\left(\frac{C+1}{C-1} \right) - \frac{2}{\ln C}}. \tag{24}$$

To investigate the negative stiffness features of disc spring, it is defined as

$$\kappa = \frac{4E}{(1-\mu^2)} \cdot \frac{t_c^4}{K1D^2}, \; x^* = \frac{x}{t_c}, \; \alpha = \frac{h_0}{t_c}.$$

By substituting them into eq. (23), the following can be obtained:

$$F_d = \kappa \left[\frac{1}{2} x^{*3} - \frac{3}{2} \alpha x^{*2} + \left(\alpha^2 + 1 \right) x^* \right]. \tag{25}$$

By conducting derivation of x at the two sides of eq. (25), the disc spring stiffness is expressed as

$$k_d = \frac{dF_d}{dx} = \frac{\kappa}{t_c} \left[\frac{3}{2} x^{*2} - 3\alpha x^* + \alpha^2 + 1 \right]. \tag{26}$$

It is demonstrated that the disc spring stiffness k_d is a quadratic function of the deformation x^*. Its symmetry axis is determined to be $x^* = \alpha$ and $k_d(0) = \lambda(\alpha^2+1)/t_c > 0$. To ensure the disc spring have a negative stiffness range, it should satisfy that $\Delta = (-3\alpha)^2 - 6(\alpha^2+1) > 0$, i.e. $\alpha > \sqrt{2}$. At that moment, the negative stiffness range is

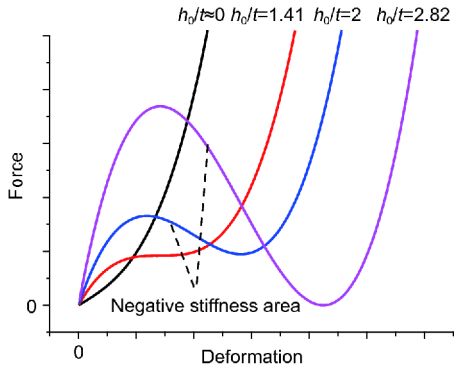

Figure 9 (Color online) Force-deformation curve of the disc spring.

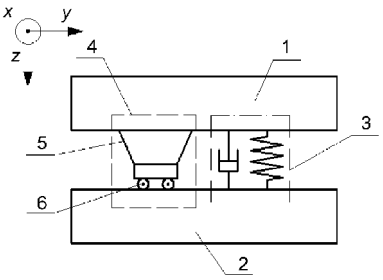

Figure 10 A schematic of a HSLDS isolators (1: car body connection end; 2: DVA connection end; 3: rubber; 4: disc spring negative stiffness structure only providing vertical stiffness; 5: disc spring; 6: sliding mechanism or lubrication layer).

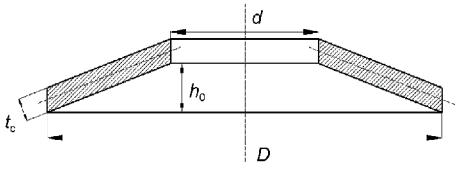

Figure 11 Cross-section schematic of disc spring.

$$\left(\frac{3\alpha - \sqrt{3\alpha^2-6}}{3}, \frac{3\alpha + \sqrt{3\alpha^2-6}}{3} \right).$$

The vertical stiffness-displacement curve of the HSLDS isolator is displayed in Figure 12, where k_{aopt} is the optimum design value of the DVA vertical stiffness, as follows:

$$k_{aopt} = (2\pi f_{opt})^2 m_e / n, \tag{27}$$

where f_{opt} is the vertical optimal natural frequency of the device, m_e is the mass of the DVA, and n is the number of HSLDS isolators. Furthermore, k_d is the disc spring vertical stiffness-displacement curve calculated by eq. (26), k_z is the vertical stiffness of the paralleled rubber isolators, and k_a is the vertical stiffness of the HSLDS isolator, as follows:

$$k_a = k_z + k_d = k_z + \frac{\kappa}{t_c} \left[\frac{3}{2} \frac{x}{t_c}^2 - 3\alpha \frac{x}{t_c} + \alpha^2 + 1 \right]. \tag{28}$$

As shown in Figure 12, when the system vibrated around the equilibrium position, the vertical stiffness of the HSLDS

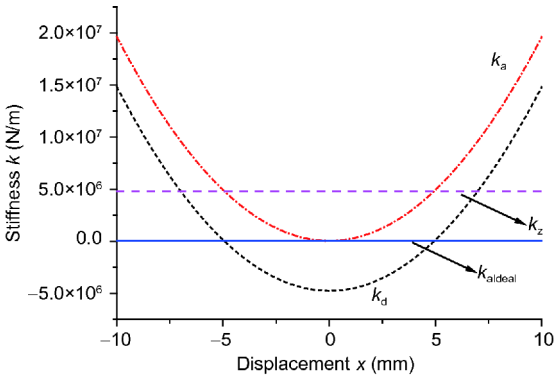

Figure 12 (Color online) The vertical stiffness-displacement curve of the HSLDS isolator.

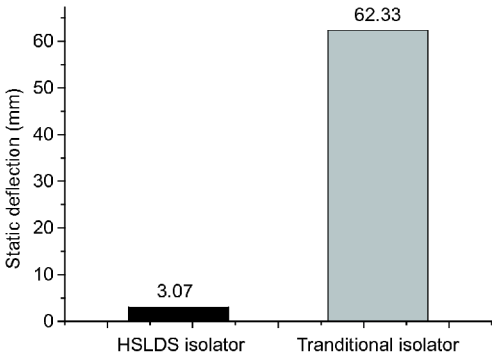

Figure 13 (Color online) The static deflection comparison diagram.

isolator k_a reached the optimum designed value of vertical stiffness k_{aopt}. At that moment, the static deflection of the DVA is $\delta_{st}=(m_c g/n-F_d(0))/k_z$. The static deflection comparison of HSLDS isolator and tranditional linear isolator is shown in Figure 13. As can be seen from the figure, the traditional isolator due to static deflection is too large for such a low frequency suspension.

5 Vibration performance validation of the HSLDS isolators by a simulation model

In Sect. 2, the vibration performance of the 2DOF DVA on car body is analyzed, during which the suspension stiffness is set as linear stiffness. But the stiffness of HSLDS isolators is nonlinear. To verify vibration reduction performance of HSLDS isolators, a nonlinear vehicle dynamics model is established by the multibody system simulation tool SIMPACK, which is shown in Figure 14. The effect of 2DOF DVA on vehicle vibration performance is discussed by time integral calculation. The track irregularity also uses high-speed high excitation spectrum shown in Figure 4.

Figure 15 shows the comparison of the vibration acceleration PSD at the car body middle by the SIMPACK model with that by the linear model in Sect. 2. As can be seen, the calculated results of the two models are in good agreement in all frequency range, especially in the range of the floating mode frequency of the car body (around 0.678 Hz).

Table 3 shows the comparison of the car body vibration modal frequency and damping ratio of the linear model in Sect. 2 and the SIMPACK model. As can be seen, the calculated results of the two models are in good agreement.

Currently, high-speed train commonly adopt light-weighting technology. It is unpractical to suspend tons of DVA under a car body. One possible way to apply them is to regard under-chassis-suspended device as a DVA. For a specific train system, the mass and rotational inertia of its under device are usually identified. Adjustments can only be made according to suspension stiffness and damper. Figure

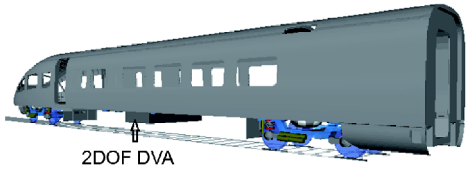

Figure 14 (Color online) The vehicle model by SIMPACK.

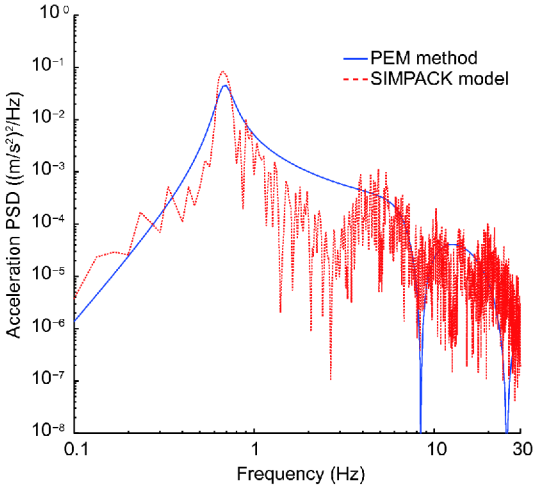

Figure 15 (Color online) The acceleration PSD at the car body middle (350 km/h).

16 shows the influence of suspension stiffness on the car body bouncing acceleration PSD based on 4 mounting points are applied. When the suspension stiffness is 27 kN/m, the under-chassis-suspended equipment achieves the optimal value of bouncing vibration. At that moment, the car body bouncing vibration acceleration amplitude is the lowest.

6 Conclusions

In this paper, a high-speed train vertical linear dynamics model isestablished, and a 2DOF low frequency DVA mechanism is proposed based on acceleration. The aim of this

Table 3 Comparison of the car body vibration modal frequency and damping ratio

Order	Vibration mode	Linear model (Sect. 2)		SIMPACK model	
		Frequency (Hz)	Damping ratio (%)	Frequency (Hz)	Damping ratio (%)
1	Car body bouncing	0.6782	10.51	0.6831	10.52
2	Car body pitching	0.8992	13.98	0.9102	14.02
3	Bogie reverse bouncing	6.9271	30.74	7.0681	30.82
4	Bogie homonymous bouncing	6.9343	30.61	7.0855	30.78
5	Leading bogie pitching	12.3947	45.41	12.5851	45.85
6	Trailing bogie pitching	12.3947	45.41	12.5851	45.85

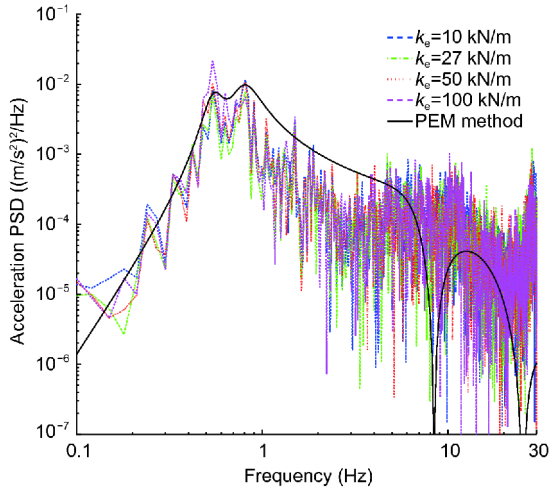

Figure 16 (Color online) Influence of suspension stiffness on the car body bouncing PSD.

mechanism is to control bouncing and pitching of the car body which are low frequency. By PEM and covariance algorithm, the car body vibration acceleration PSD and Sperling Index are calculated. The results indicate that after adopting the 2DOF low frequency DVA, the main frequency of the car body bouncing vibration changes from a single-peak value to a double-peak value, and the peak value at the original bouncing vibration frequency decreases dramatically. The peak value of the car body pitching vibration also decreases. The peak values of bouncing or pitching vibration acceleration PSD at the vibration modal frequency decrease with the increase of mass or inertia ratio. Focusing on the low frequency suspension isolators required by 2DOF DVA, a HSLDS isolator with nonlinear stiffness is designed. A vehicle nonlinear dynamics model is established by SIMPACK, which is good agreement with the linear model, and the influence of the 2DOF DVA on the vehicle vibration performance is discussed. When the 2DOF DVA achieves optimum value, the reduction effect on the bouncing and pitching vibrations is the best. The results indicate that the 2DOF DVA effectively reduced car body bouncing and pitching, and increasing the vehicle ride quality.

This work was supported by the National Natural Science Foundation of China (Grant No. 51805373).

1 Yan B, Liu S, Pu H, et al. Elastic-plastic seismic response of crts ii slab ballastless track system on high-speed railway bridges. Sci China Technol Sci, 2017, 60: 865–871
2 Zhang Y D, Zhang J Y, Li T, et al. Investigation of the aeroacoustic behavior and aerodynamic noise of a high-speed train pantograph. Sci China Technol Sci, 2017, 60: 561–575
3 Zhou J, Shen G, Zhang H, et al. Application of modal parameters on ride quality improvement of railway vehicles. Vehicle Syst Dyn, 2008, 46: 629–641
4 Zhou J, Goodall R, Ren L, et al. Influences of car body vertical flexibility on ride quality of passenger railway vehicles. Proc Institution Mech Engineers Part F-J Rail Rapid Transit, 2009, 223: 461–471
5 Gong D, Zhou J, Sun W. On the resonant vibration of a flexible railway car body and its suppression with a dynamic vibration absorber. J Vib Control, 2013, 19: 649–657
6 Gong D, Zhou J, Sun W. Passive control of railway vehicle car body flexural vibration by means of underframe dampers. J Mech Sci Technol, 2017, 31: 555–564
7 Gong D, Zhou J, Sun W, et al. Method of multi-mode vibration control for the carbody of high-speed electric multiple unit trains. J Sound Vib, 2017, 409: 94–111
8 Shi H L, Luo R, Wu P B, et al. Application of dva theory in vibration reduction of carbody with suspended equipment for high-speed emu. Sci China Technol Sci, 2014, 57: 1425–1438
9 Dumitriu M. A new passive approach to reducing the carbody vertical bending vibration of railway vehicles. Vehicle Syst Dyn, 2017, 55: 1787–1806
10 Garg V K. Dynamics of Railway Vehicle Systems. New York: Academic Press, 1984
11 Carrella A, Brennan M J, Kovacic I, et al. On the force transmissibility of a vibration isolator with quasi-zero-stiffness. J Sound Vib, 2009, 322: 707–717
12 Carrella A, Brennan M J, Waters T P, et al. Force and displacement transmissibility of a nonlinear isolator with high-static-low-dynamic-stiffness. Int J Mech Sci, 2012, 55: 22–29
13 Carrella A, Brennan M J, Waters T P, et al. On the design of a high-static-low-dynamic stiffness isolator using linear mechanical springs and magnets. J Sound Vib, 2008, 315: 712–720
14 Huang X, Liu X, Sun J, et al. Vibration isolation characteristics of a nonlinear isolator using euler buckled beam as negative stiffness corrector: A theoretical and experimental study. J Sound Vib, 2014, 333: 1132–1148
15 Huang X, Liu X, Sun J, et al. Effect of the system imperfections on the dynamic response of a high-static-low-dynamic stiffness vibration isolator. Nonlinear Dyn, 2014, 76: 1157–1167
16 Huang X C, Liu X T, Hua H X. Effects of stiffness and load im-

perfection on the isolation performance of a high-static-low-dynamic-stiffness non-linear isolator under base displacement excitation. Int J Non-Linear Mech, 2014, 65: 32–43
17 Palomares E, Nieto A J, Morales A L, et al. Numerical and experimental analysis of a vibration isolator equipped with a negative stiffness system. J Sound Vib, 2018, 414: 31–42
18 Meng L, Sun J, Wu W. Theoretical design and characteristics analysis of a quasi-zero stiffness isolator using a disk spring as negative stiffness element. Shock Vib, 2015, 2015: 1–19
19 Meng L, Liu F. Design and analysis of a quasi-zero stiffness isolator using a slotted conical disk spring as negative stiffness structure. J Vibroeng, 2014, 16: 1769–1785
20 Seto K. Dynamic Vibratin Absorber and Its Applications. Beijing: China Machine Press, 2013
21 Liu K, Liu J. The damped dynamic vibration absorbers: Revisited and new result. J Sound Vib, 2005, 284: 1181–1189
22 Zhou J S. Vibration and Control of Railway Vehicles. Beijing: China Railway Publishing House, 2012
23 Lin J H, Zhang Y H, Zhao Y. Pseudo excitation method and some recent developments. Procedia Eng, 2011, 14: 2453–2458
24 Lin J, Zhang W, Li J. Structural responses to arbitrarily coherent stationary random excitations. Comput Struct, 1994, 50: 629–633
25 Zhang Y. Spring Manual. Beijing: China Machine Press, 1997